AIMS Materials Science, 3(4): 1410-1425.
DOI: 10.3934/matersci.2016.4.1410
Received: 15 August 2016
Accepted: 20 October 2016
Published: 24 October 2016

http://www.aimspress.com/journal/Materials

Research article

High-performance photocatalyst based on nanosized ZnO-reduced graphene oxide hybrid for removal of Rhodamine B under visible light irradiation

Haiqing Yao [1,2], Fei Li [3], Jodie Lutkenhaus [3], Masaya Kotaki [4], and Hung-Jue Sue [1,2,*]

[1] Department of Materials Science and Engineering, Texas A&M University, College Station, TX 77843, USA
[2] Polymer Technology Center, Texas A&M University, College Station, TX 77843, USA
[3] Artie McFerrin Department of Chemical Engineering, Texas A&M University, College Station, TX 77843, USA
[4] Kaneka US Material Research Center, College Station, TX 77843, USA

* **Correspondence:** Email: hjsue@tamu.edu.

Abstract: Nano-sized zinc oxide-reduced graphene oxide (ZnO-RGO) hybrid containing well-dispersed ZnO nanoparticles with an average diameter of 4.5 ± 0.5 nm has been successfully prepared via a one-step sol-gel method. FTIR characterization reveals that GO underwent deoxygenation during the preparation of ZnO nanoparticle. The introduction of RGO in the ZnO-RGO hybrid significantly improved the photocatalytic efficiency of ZnO in the degradation of Rhodamine B under visible light irradiation. The apparent reaction constant of ZnO-RGO is 8 times higher than that of pure ZnO, and the photocatalytic efficiency of ZnO-RGO remains high even after 4 consecutive reactions. Results from the X-ray photoelectron spectroscopy, Brunauer-Emmett-Teller surface area measurements, and electrochemical impedance spectroscopy analysis suggest that the enhancement in the photocatalytic activity of the ZnO-RGO hybrid comes from (1) the enormous surface area provided by the nano-sized ZnO particles, (2) significant dye adsorption from RGO template, and (3) excellent electron reception and conduction of RGO. The attractive properties of ZnO-RGO make it a promising candidate material in addressing the environmental pollution issues we have to face today.

Keywords: reduced graphene oxide; ZnO; sol-gel; photocatalysis; adsorption

1. Introduction

Photocatalytic degradation of organic pollutants by semiconducting metal oxides (especially TiO_2 and ZnO) has received increasing attention during the past decade as a promising technology for pollution abatement [1,2,3]. Both ultraviolet (UV) and visible light irradiation can activate photocatalysis [4]. The UV light irradiation mechanism involves the excitation of the semiconductor with a concomitant generation of a variety of reactive oxidation species (ROS, such as $\cdot O_2^-$, HOO· and ·OH). Subsequently, photo-oxidation of the organic pollutants by these species can take place, and the pollutants can be degraded into harmless mineralized products or water and CO_2. In the case of visible light, one of the photocatalytic mechanisms is dye-sensitized photocatalysis. This mechanism involves the excitation of the pollutants instead of the semiconductor, followed by electron transfer from the excited pollutants to the conduction band of the semiconductors. The injected electron reacts with the surface-adsorbed O_2 molecules to yield ROS. Then, these reactive species degrade the organic pollutant into mineralized products. Dye-sensitized photocatalysis through visible light is more economic than UV light, because visible light makes up a larger portion of sunlight and can also be effective in indoors environments [4]. However, synthesis of highly active, effective dye-sensitized photocatalysts by visible light remains scarce.

An ideal visible light-active photocatalyst needs good electron transfer from the organic pollutant to the semiconductor and a slow electron-hole pair recombination. Several attempts have been made to enhance charge transport and separation, including conjugation of the semiconductor with electron scavenging agents, like heterogeneous atoms/ions and electron-accepting materials [5–10]. For the latter, graphene has been recognized as one of the most promising materials for supporting photocatalytic semiconductors because of its unique electronic properties and large surface area [3,6,11,12]. It has been demonstrated that graphene surfaces decorated with various kinds of nanoparticles, such as Au, Pt, and TiO_2, display high activity for catalytic applications [6,13–18]. These advanced functions can be attributed to the huge surface area and the excellent electron conduction properties of graphene. Therefore, the combined usage of graphene and semiconductors offers promising potential for effective photodegradation of organic pollutants into environmentally benign species by visible light [19,20,21]. Graphene can be prepared via reduction of graphene oxide (GO) such as chemical reduction using hydrazine or $NaBH_4$ and high temperature annealing reduction [22,23]. However, in most of the reported methods, hazardous reducing agents under high temperature or long processing time are required to achieve reasonable reduction. Another problem with reduced graphene oxide (RGO) is that the strong inter-sheet van der Waal interactions cause RGO to form irreversible agglomeration or even restack to form graphite. This poses a great challenge to exploiting graphene properties for photocatalytic applications. Thus, a simple and straightforward method is needed to prepare nanoparticle and RGO hybrids that retain the RGO exfoliation for optimal photo-catalytic performance.

Among the various semiconductor photocatalysts, ZnO has attracted great attention because of its wide band gap (3.37 eV), high electron mobility, low cost, and environmental friendliness [9,24]. Recently, progress has been made to prepare ZnO-graphene hybrids [7,25,26,27]. Li et al. reported a chemical deposition method to prepare ZnO-graphene hybrids, and the as-prepared ZnO nanoparticles had diameters ranging from 10–20 nm [7]. A hydrothermal approach was also reported to fabricate ZnO nanorod-graphene hybrids by Chen and his coworkers [26]. The length and diameter of blank ZnO nanorods are ca. 50–200 nm and 15–30 nm, respectively. Li et al. reported a facile strategy to synthesize ZnO-graphene in water consisting of flower-like ZnO nanoparticles with diameters of about 1 μm [27]. Although these ZnO-graphene hybrids have shown outstanding performance as photocatalysts, the particle sizes for ZnO in these reports are still too large. Further reduction in ZnO sizes is likely to improve the photocatalytic activity of the catalysts [28]. There are two main attributes related to the quantized ZnO nanoparticles: quantum confinement effect and large surface-to-volume ratio [29]. For the quantum confinement effect, the band gap of a semiconductor increases and the band edges shift to yield larger redox potentials as the particle diameter falls below a critical radius of approximately 7 nm for ZnO [29,30]. The increased driving force in size-quantized systems is expected to increase the rate constant of charge transfer [31]. Secondly, the large surface-to-volume ratio of quantized particles is expected to provide a large overall contact surface area with graphene and lead to an efficient hybridization with graphene. Such a hybridization effect would retard the recombination of electron-hole pairs and inhibit photocorrosion of ZnO nanoparticles, which should lead to an enhanced photoactivity [32]. Therefore, it is important to reduce the ZnO particle sizes to below 7 nm to exert quantum confinement effect to achieve an optimal synergetic effect from both ZnO and graphene.

In this work, we report a simple and straightforward approach to prepare ZnO-RGO via a one-step reaction. GO was directly reduced into RGO during the preparation of ZnO without using additional reducing agents. The as-prepared ZnO-RGO hybrid contains exfoliated RGO and well-dispersed, nanometer-sized ZnO nanoparticles anchored on RGO with an average diameter of 4.5 ± 0.5 nm. This synthesis method provides an efficient and economic approach toward achieving high quality graphene-based nanocomposites. During the reaction, graphene sheet serves as a 2D template for the anchoring, nucleation, and growth of soluble ZnO precursor into ZnO nanoparticles. Thus, sufficient interfacial interaction exists between ZnO and RGO. Furthermore, RGO also plays a key role for the photocatalytic process. The ZnO-RGO hybrid shows superior performance for the photodegradation of Rhodamine B under visible light irradiation. Possible mechanisms for the observed enhancement in photocatalytic activity are discussed.

2. Materials and Methods

2.1. Materials

Graphite (SP-1 graphite, average particle sizes of 45 μm) was obtained from Bay Carbon Inc, USA. Zinc acetate dihydrate, potassium hydroxide, Rhodamine B, sulfuric acid, sodium nitrite, potassium permanganate, and methanol were purchased from Sigma-Aldrich and were used as received.

2.2. Synthesis of ZnO Nanoparticles

ZnO nanoparticles were prepared by hydrolyzing zinc acetate dihydrate in methanol. This method has been previously reported [33]. KOH (1.0 g, 17.8 mM) was first dissolved in 200 mL methanol at 70 °C with refluxing and stirring to obtain a homogeneous solution. Subsequently, zinc acetate dihydrate (2.0 g, 8.9 mM) methanol solution (22 mL) was added directly into the basic methanol solution. This mixture was then kept at 70 °C with refluxing and stirring for 2 hours. The prepared ZnO nanoparticles were purified by the precipitation and dispersion procedure twice.

2.3. Synthesis of ZnO-RGO Hybrids

GO was prepared by the Hummers' method [34]. Graphite powder (0.5 g) was firstly treated with a solution containing concentrated H_2SO_4 (50 mL) and $NaNO_3$ (0.5 g) below 5 °C. $KMnO_4$ (3 g) was added gradually, and the mixture was stirred continuously for 2 h. The mixture was then kept at 35 °C for another 2 h. The mixture was diluted with deionized (DI) water (23 mL) and stirred for 15 min. Additional DI water (71 mL) and 30% H_2O_2 (10 mL) were added to the mixture, which changed the mixture's color to brilliant yellow. Finally, the mixture was washed with water several times and HCl once to remove metallic ions.

The method to synthesize ZnO-RGO hybrid is similar to that of ZnO nanoparticles. GO (80 mg, 0.8 mg/mL) was mixed with a KOH (0.5 g, 8.9 mM) methanol solution and sonicated for 30 minutes to obtain a homogeneous solution, and then heated to 70 °C for 15 min. After that, a zinc acetate dihydrate (1 g, 4.5 mM) methanol solution (11mL) was added, and the mixture was kept stirring for 2 hours at 70 °C. The ZnO-RGO hybrids were filtered through a membrane with 0.5 μm pore size to remove ungrafted ZnO nanoparticles.

2.4. Characterization

Fourier transform infrared spectroscopy-attenuated total reflectance (FTIR-ATR) spectra of the samples were acquired using Nicolet 380 (Thermo Fisher Scientific) in conjunction with ATR accessory (AVATAR OMNI Sampler, Germanium crystal) under ambient condition. Transmission electron microscopy (TEM) images were obtained from a JEOL 2010 high-resolution microscope operated at 200 kV. X-ray photoelectron spectroscopy (XPS) data was obtained with a Kratos Axis Ultra using a non-monochromatic MgK_α photon source (1486 eV) for measurements. X-ray diffraction (XRD) patterns of ZnO and ZnO-RGO were acquired using a Bruker D8 Advanced Powder X-ray Diffractometer with CuK_α incident radiation (k = 1.5418 Å). Thermal gravimetric analysis (TGA) of ZnO-RGO hybrids was performed with ~8 mg of solid powder. The test was run from 30 °C to 900 °C with a ramp rate of 20 °C/min in air. UV-Vis absorption spectra were acquired with a UV-Vis-NIR spectrophotometer (Shimadzu, UV-3600). The Brunauer-Emmett-Teller (BET) surface area measurements were performed on a Beckman Coulter SA 3100 surface area and pore size analyzer at 77 K with prior degassing under vacuum at 80 °C for 2 hours.

2.5. Photocatalytic Activities of ZnO and ZnO-RGO

The photodegradation of Rhodamine B (RhB) was carried out under visible light irradiation. In a typical process, catalyst (5 mg) was suspended in RhB aqueous solution (3×10^{-5} M, 3 mL). To best match the sun-like emission, the solution was exposed to the visible light irradiation produced by a solar simulator positioned 20 cm away from the container. The 260 W Xe lamp produces a sun-like emission spectrum. To rule out the impact of UV light, the Xe lamp was covered by a UV filter sheet (CON-TROL-CURE® RIGID UV filter sheets). It can filter out 100% of UV light below 390 nm and 98% between 390 nm and 400 nm. The degraded solution was analyzed by UV-Vis spectroscopy at predetermined time intervals. The long-term effectiveness of the catalyst was tested as follows: ZnO-RGO (8 mg) was dispersed in RhB aqueous solution (3×10^{-5} M, 5 mL), and the solution was exposed to the visible light irradiation for 20 min. The catalyst underwent four consecutive cycles and was centrifuged and washed thoroughly with water after each cycle.

2.6. Fabrication of the Electrodes for Electrochemical Impedance Spectroscopy (EIS) Measurements

For the EIS measurement, the catalyst (5.0 mg) was dispersed in 1.0 mL methanol, and the solution was then dropped on the conducting fluorine doped tin oxide (FTO) glass substrate (24 Ω/square). Impedance measurements (Interface 1000, Gamry Instruments) were carried out at room temperature. The catalyst-coated FTO served as the working electrode, with a platinum wire and aqueous Ag/AgCl as the counter and reference electrode, respectively. The supporting electrolyte was a 2.5 mM $K_3[Fe(CN)_6]/K_4[Fe(CN)_6]$ (1:1) mixture as redox probe in a 0.1 M KCl solution. The impedance spectra were recorded using amplitude of 5 mV over the frequency range of 0.1–10^5 Hz.

3. Results and Discussion

3.1. Characterization of ZnO-RGO Hybrids

The procedure for the synthesis of ZnO-RGO in methanol is illustrated in Figure 1. Firstly, GO was heated at 70 °C to mix with potassium hydroxide in methanol for a 15 minutes and this procedure was accompanied by a fast color change from yellowish brown to black (Figure S-1). This color change indicates GO underwent a fast reduction process under alkaline solution, which agrees with the literature report [35]. Further evidence could be found in the FTIR analysis as shown in Figure 2. The nucleation of ZnO happened when zinc acetate dehydrate was added in the mixture. During the reaction, RGO sheet serves as a 2D template for the anchoring, nucleation, and growth of soluble ZnO precursor into ZnO nanoparticles. The in-situ growth of ZnO on RGO surface is beneficial for direct interaction between soluble precursor and RGO, where the residual oxygen functional groups on RGO would attract zinc ions to form ZnO. The further growth of ZnO precursor into ZnO would prevent the RGO from restacking.

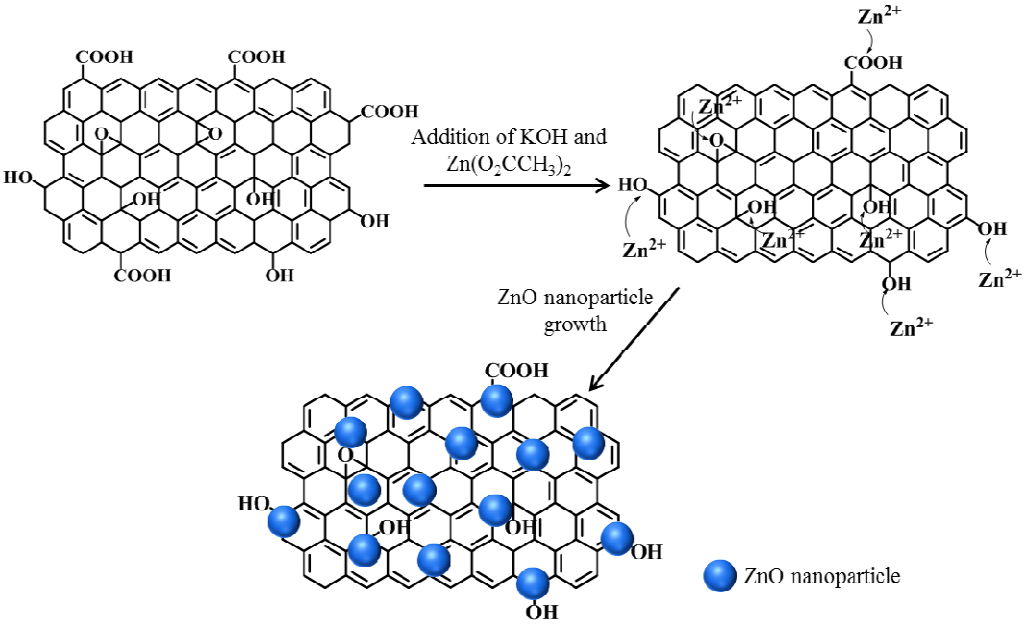

Figure 1. Illustration of ZnO-RGO nanohybrids preparation.

The chemical reduction process of GO through the in-situ growth of ZnO nanoparticle was characterized by FTIR. To well understand the reduction mechanism, RGO suspension obtained from direct mixing GO with potassium hydroxide under heat at 70 °C for 15 minutes was also prepared [35]. To rule out the signal from extra KOH, the RGO suspension was purified through filtration and washed with DI water. As shown in Figure 2, GO shows the typical peaks at 3436, 1735, 1621, and 1050 cm^{-1}, which correspond to the hydroxyl groups, carboxyl groups, π-π structure and carbon oxygen bond, respectively. After mixing with potassium hydroxide, RGO shows a significant decrease in the intensity of carboxyl group peak (1735 cm^{-1}). The same change is also found on ZnO-RGO. This indicates that GO underwent a fast oxygen reduction process even before the growth of ZnO nanoparticle. This interesting reaction provides a feasible route to the preparation of ZnO-RGO hybrids. Although the underlying reaction mechanism between GO and alkaline solution is still unclear, it has been reported that the chemical reduction of GO is indeed pH dependent. That is, the higher the pH of the suspension, the faster the reaction will become [13,35].

The morphologies of GO and the resultant ZnO-RGO were characterized by TEM. As shown in Figure 3a, a typical 2D GO sheet by itself shows a wrinkled structure. After the growth of ZnO nanoparticles on the graphene surface, the graphene did not change in morphology. The TEM images of the ZnO-RGO hybrid (Figure 3b and 3c) clearly indicate that spherical ZnO nanoparticles are anchored and well distributed on the graphene surface. TEM images of pure ZnO nanoparticles with a diameter of ~5 nm are shown in Figure S-2. From a statistical analysis of particle size based on 100 nanoparticles, the ZnO nanoparticles on graphene sheets have an average particle size of 4.5 ± 0.5 nm (Figure 3d). This result is consistent with the particle size calculated from its band gap energy, determined experimentally from the optical absorption onset in the UV-Vis spectrum (Figure S-2) [30]. Pure ZnO and ZnO-RGO in methanol have the same absorption onset at 359.0 nm, which is blue-shifted when compared to that of the bulk ZnO of 3.35 eV at room temperature.

According to the effective mass model [36], ZnO with a particle size of 5 nm yields the band gap energy E* of 3.45 eV. These results indicate that the presence of graphene does not change the growth process of ZnO nanoparticles and ZnO nanoparticles exhibit the same crystalline structure and diameter after in situ growth on graphene surface.

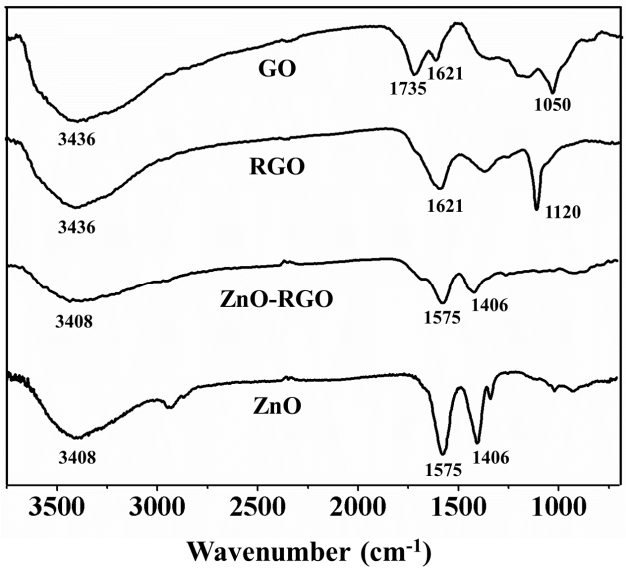

Figure 2. FTIR characterization of GO, RGO, ZnO-RGO and ZnO.

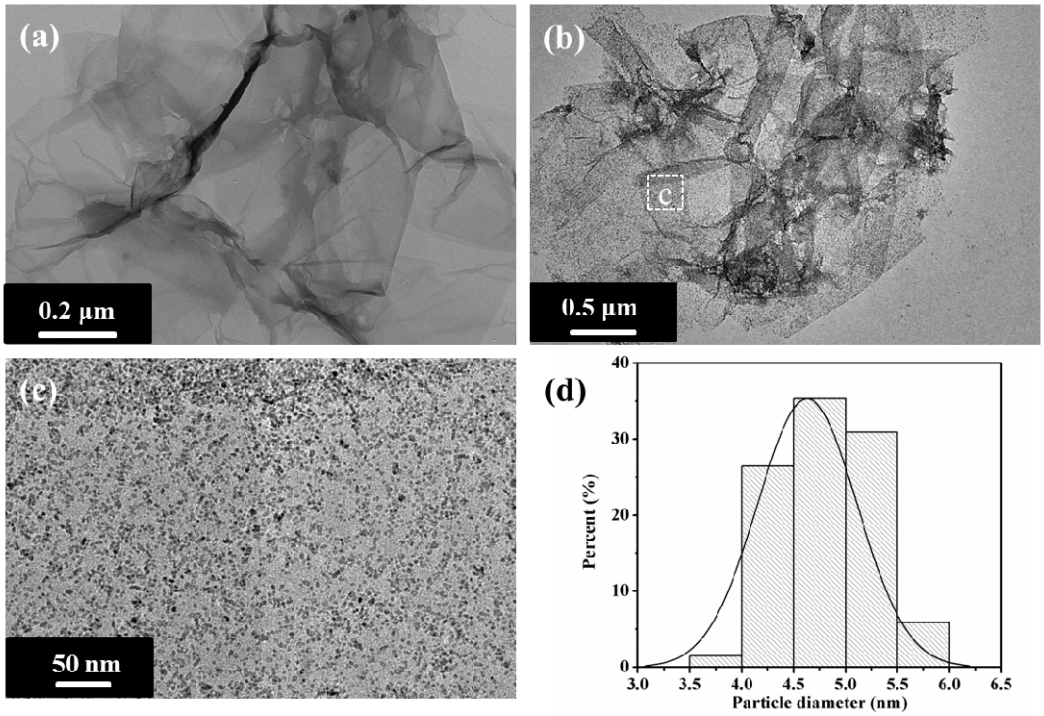

Figure 3. TEM images of (a) GO, (b) ZnO-RGO, (c) high magnification of ZnO-RGO shown in area in (b), and (d) ZnO size distribution in ZnO-RGO.

The chemical species of the ZnO-RGO were studied by XPS. As shown in Figure 4a, the Zn peaks are dominant. However, C and O peaks also appear. The peaks located at 284 and 531 eV are attributed to C 1s and O 1s [37]. The remaining peaks at higher binding energies (1045 and 1022 eV) are assigned to Zn 2p1/2 and 2p3/2, respectively [7]. The XRD patterns of GO, ZnO, and ZnO-RGO are shown in Figure 4b. ZnO and ZnO-RGO both present diffraction peaks at 2θ = 31.7°, 34.3°, 36.1°, 47.4°, 56.4°, 62.91°, and 67.9°, corresponding to the wurtzite ZnO structure of (100), (002), (101), (102), (110), (103) and (112) reflections, respectively [33]. GO displays a sharp peak at 2θ = 10.2°, with a d-spacing of 0.87 nm. The crystalline peak of graphite appears at 26.2°, which is the characteristic peak of hexagonal graphite with a d-spacing of around 0.34 nm [26]. The expansion in the interlayer spacing of GO is an indication of the absorbed water and oxygen functionalities among the GO interlayers. However, no characteristic peak is observed on the XRD pattern of ZnO-RGO in the corresponding regions. This may be due to the presence of anchored ZnO nanoparticles, which disrupts the RGO sheets from forming stacks.

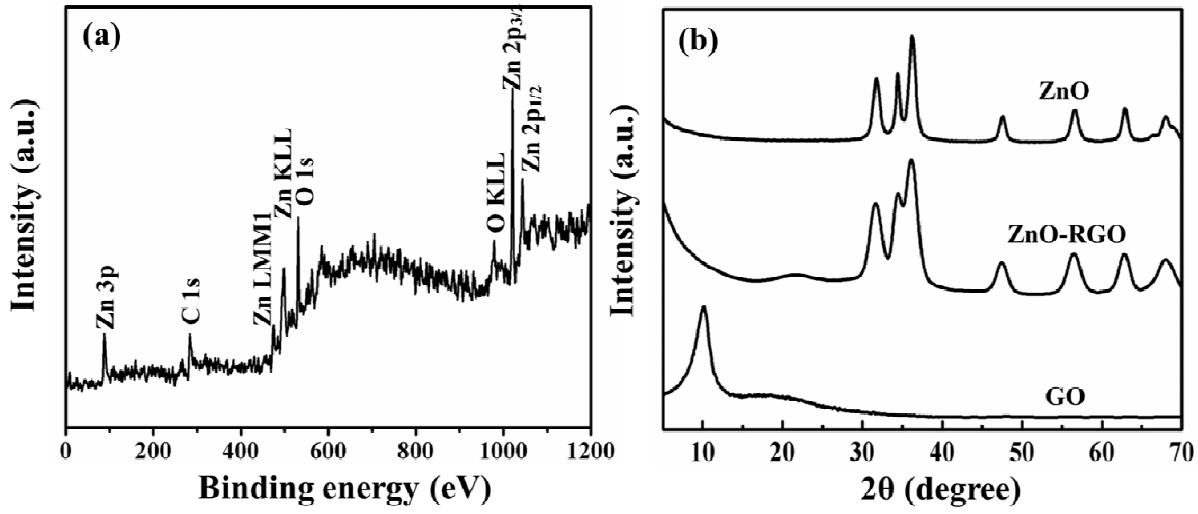

Figure 4. (a) XPS spectrum of ZnO-RGO, (b) XRD patterns of ZnO, ZnO-RGO and GO.

The chemical content of the ZnO-RGO is calculated from TGA results (Figure 5 and S-3). Two thermal degradation processes are shown in the TGA curve of ZnO. The degradation that happened at a temperature below 100 °C corresponds to the adsorbed methanol in ZnO. Another weight loss (~5 wt%) was observed in the temperature range of 250–350 °C. This loss is due to acetate ligands bound to the surface defects of the nanoparticles [33]. The TGA trace of ZnO-RGO shows multiple weight losses in the temperature range of 30 to 400 °C. The weight loss from 30 to 150 °C is due to the absorbed solvent between graphene layers. The decomposition of the oxygen groups on graphene occurs at 150–250 °C. The weight loss above 250 °C is attributed to the oxidation of graphene under air. Based on the above finding, the content of graphene in ZnO-RGO could be calculated from these TGA curves to be roughly 10 wt%.

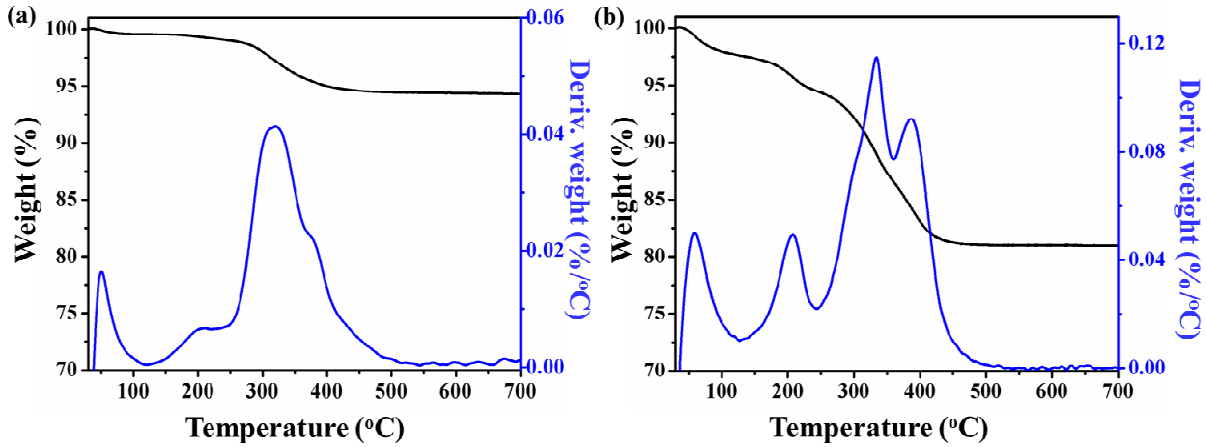

Figure 5. TGA curves and the corresponding derivatives of (a) ZnO and (b) ZnO-RGO.

3.2. Photocatalytic Characterization of ZnO-RGO

The photocatalytic activities of ZnO and ZnO-RGO were determined by photodegradation of Rhodamine B (RhB) as a model reaction under visible light. The temporal evolution of the spectral changes during the photosensitized degradation of RhB in the presence of ZnO and ZnO-RGO is shown in Figure 6. In general, in the presence of ZnO and ZnO-RGO catalysts, visible light irradiation of the aqueous RhB solution leads to a decrease in its UV-Vis absorption with time. However, these two catalysts give different photodegradation efficiencies. ZnO shows a rather poor photocatalytic activity. Only 28% of RhB is decomposed in 16 min, and it takes 100 min for the complete degradation of RhB. In contrast, ZnO-RGO photocatalyst exhibits remarkable improvements in the photodegradation of RhB, with 100% of the dye molecules degraded in 16 min. Note that there is no obvious peak wavelength shift for both ZnO and ZnO-RGO systems with increasing time. This indicates that the photodegradation of RhB is dominated by the degradation of the aromatic chromophore but not the de-ethylation of RhB [4,16]. It should be noted that without presence of catalyst, the photodegradation rate of RhB is extremely slow. As shown in Figure S-5, only 46% of RhB were degraded after 120 min.

The normalized temporal concentration changes (C/C_0) of RhB during the photodegradation were derived from its normalized absorbance (A/A_0) (at 550 nm) at a given time interval. It is clear from Figure 6c that ZnO-RGO shows significantly higher photocatalytic activity than ZnO alone. The apparent reaction constants of ZnO and ZnO-RGO were calculated through pseudo first-order kinetics [38]:

$$\ln\left(\frac{c}{c_o}\right) = K_{app}t$$

where C is the concentration of RhB at time t, C_o is the initial concentration, and K_{app} is the apparent reaction constant. As shown in Table 1, pure ZnO nanoparticles exhibit a K_{app} of 0.026 min^{-1}, whereas the K_{app} of ZnO-RGO reaches into 0.202 min^{-1}, which is almost 8 times higher than that of pure ZnO.

The long-term effectiveness of ZnO-RGO for the degradation of RhB under visible light was also investigated (Figure 6d). The photodegradation of RhB was monitored for four consecutive cycles, each for 20 min. After each cycle, the photocatalysts were recovered through centrifugal separation, washed thoroughly with water and added into fresh RhB solution for the next cycle of reaction. The experimental results indicate that the ZnO-RGO still retains 70% activity for degradation of RhB after 4 consecutive uses. One possible reason for the activity decrease is the materials lost during washing processes between cycles. Due to the low photocatalytic efficiency of ZnO, there is only 29% of RhB degraded during the first cycle. After four consecutive uses, ZnO only retains 13% activity. This indicates that the incorporation of RGO in the catalyst not only increases the photocatalytic efficiency but also improves their stability during photocatalytic reaction. Most importantly, it indicates that these highly active ZnO-RGO photocatalysts can be easily separated and recovered by sedimentation, making it attractive for practical application of removing organic pollutants from the environment.

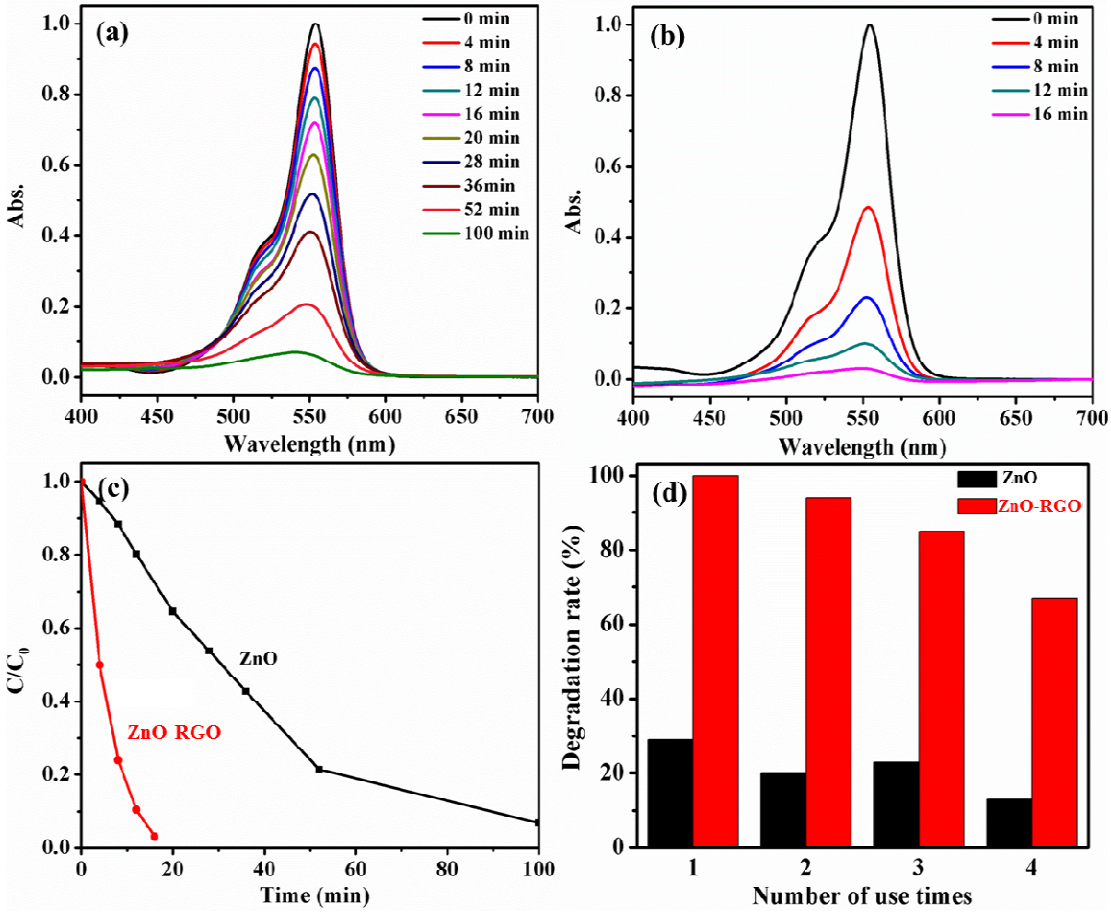

Figure 6. (a) and (b) UV-Vis spectral changes of RhB (3×10^{-5} M) as a function of time in the presence of ZnO and ZnO-RGO, (c) photocatalytic degradation of RhB in the presence of catalysts ZnO and ZnO-RGO, and (d) degradation rate of RhB in the presence of catalysts ZnO and ZnO-RGO.

Table 1. Summary of reaction rate, half-life time, surface area, and adsorption RhB under dark condition of the photocatalysts ZnO and ZnO-RGO for comparison.

Samples	K_{app} (min^{-1})	$t_{1/2}$ (min)	Surface area (m^2/g)	Adsorption of dye (%)
ZnO	0.026	25	29	5
ZnO-RGO	0.202	3	181	31

3.3. Mechanism for Enhanced ZnO-RGO Photocatalytic Activity

The photocatalytic activity of the ZnO-RGO hybrids is intrinsically governed by the ZnO particle size, the adsorption of dyes, and charge carrier mobility [3,16,32,39,40]. From TEM results, ZnO nanoparticles on the graphene surface have an average particle size of 4.5 ± 0.5 nm, which is smaller than the particle sizes in most reports [7,26,27]. Increased photocatalytic efficiency for ZnO is expected. Owing to the quantum confinement effect, the band gap of ZnO increases and the band edges shift to yield larger redox potentials [31]. The increased redox potential in size-quantized systems is expected to increase the rate constant of charge transfer. Furthermore, the large surface-to-volume ratio can provide ample contact surface area of ZnO with RGO and lead to efficient hybridization. The hybridization effect can be verified by the high-resolution XPS spectra of Zn 2p3/2 for ZnO and ZnO-RGO (Figure 7a). The spectrum for the ZnO sample reveals that the core Zn 2p3/2 peak is positioned at 1021.4 eV with high symmetry, indicating that Zn was present only in the Zn^{2+} state [41]. However, the Zn 2p3/2 peak of ZnO-RGO exhibits a shift to a higher binding energy by 2.4 eV. The shift to higher binding energy signifies an increased oxidation of Zn, resulting from its contact with the electronegative graphene [42]. This indicates that the electronegative graphene surfaces create a stronger dipole moment with ZnO nanoparticles. Such a hybridization effect can retard the recombination of electron-hole pair and inhibit the photocorrosion of ZnO nanoparticles [32]. Therefore, the synergetic effect of quantum confinement and large surface-to-volume ratio from quantized ZnO particles contributes to the enhanced photodegredation of RhB.

Another factor for the enhanced photocatalytic activity of ZnO-RGO is the enhanced adsorption of dyes by RGO. The adsorption characteristics of RhB onto the surface of both ZnO and ZnO-RGO were investigated. The concentrations of RhB after dark adsorption were obtained from UV-Vis absorption measurements. After equilibrium in the dark for 20 min, only 5% of RhB was adsorbed on the ZnO nanoparticle surface, whereas a large amount of dye molecules (ca. 31%) was adsorbed on the surface of the ZnO-RGO (Table 1). To verify the adsorptivity differences, the BET surface areas of ZnO and ZnO-RGO were characterized by N_2 adsorption-desorption at 77 K (Figure S-4). After the introduction of RGO, the BET surface area of ZnO-RGO greatly increases from 29 m^2/g of pure ZnO to 181 m^2/g, which is six times higher than that of the pure ZnO (Table 1). From these experimental results, it can be deduced that the high adsorptivity of RhB on ZnO-RGO originates from the 2D planar structure of RGO. The introduction of RGO not only retains the individual dispersion of the nanosized ZnO particles but also provides a π-π platform for adsorbing dye

molecules [9]. RhB molecule has an aromatic chromophore, which leads to a face-to-face adsorption on the RGO surface via π-π interaction. Under light irradiation, the dyes are excited and the photogenerated electrons could easily transfer to the RGO surface and then participate in the redox reaction with ZnO nanoparticles. Subsequently, the excited dye decomposes into CO_2 and H_2O through a series of redox reactions. Therefore, the synergetic effect between adsorptivity and photoreactivity is achieved in a simple process, resulting in an appreciable improvement in photodegradation of RhB compared with pure ZnO alone.

In addition to enhancing adsorptivity, RGO also serves as an electron acceptor and conductor due to its two-dimensional conjugation structure. In this aspect, RGO helps suppress charge recombination, enhancing charge separation efficiency, and improving the photocatalytic activity. The electrochemical impedance spectroscopy (EIS) of ZnO and ZnO-RGO electrodes was performed to verify the enhancement in charge transfer, and their corresponding Nyquist plots are shown in Figure 7b. With the introduction of 10 wt% of graphene, the semicircle size in the plot of ZnO-RGO becomes much smaller than that of ZnO, almost one fourth of the size of ZnO plot. The decreased semicircle size indicates an effective separation of photogenerated electron-hole pairs and faster interfacial charge transfer from the electron donor to electron receptor [43,44].

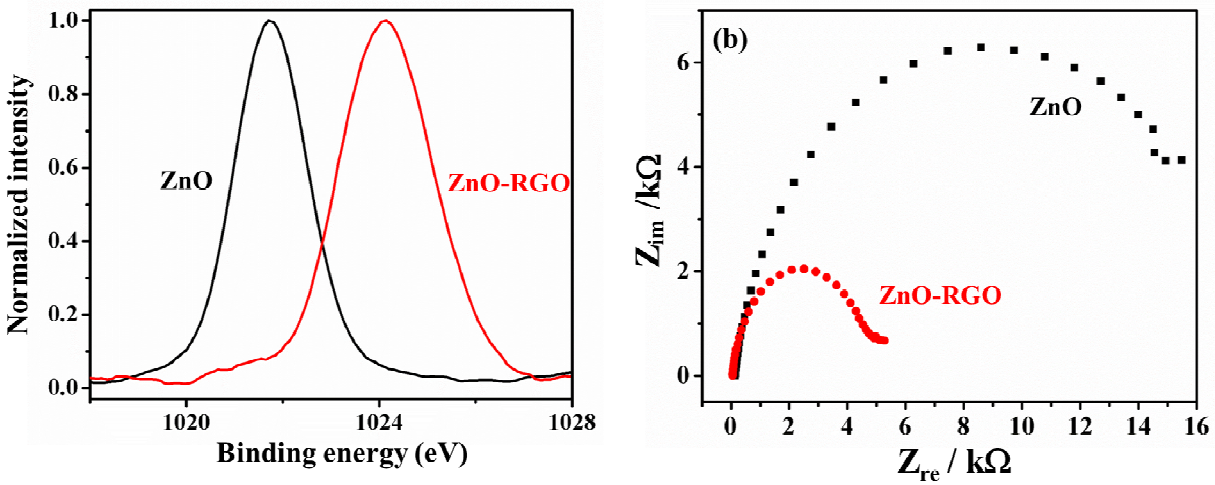

Figure 7. (a) XPS spectra of Zn 2p3/2 peak in ZnO and ZnO-RGO, and (b) EIS plots of ZnO and ZnO-RGO electrodes.

From the above-mentioned experimental findings, it can be concluded that the significant enhancement in the photocatalytic activity of ZnO-RGO comes from the following factors: nanosized ZnO particles, high dye adsorptivity of RGO, and excellent electron conduction of RGO. A schematic highlighting the mechanisms responsible for the observed enhancement in photocatalytic properties of the ZnO-RGO is given in Figure 8. Firstly, RhB molecules form a face-to-face adsorption on the RGO surface via π-π interaction. Then, under visible light irradiation, the photogenerated electrons from dyes move freely onto the surface of RGO and transfer to the nearest ZnO nanoparticles. Subsequently, the injected electron reacts with the surface-adsorbed O_2 molecules to yield ROS. Finally, the dye* degrades into mineralized products by these reactive species. The main reason for the observed excellent performance comes from the synergistic effect

from both nanosized particles and strong interaction between ZnO and RGO. Therefore, the hybridization of nano-sized ZnO with RGO in this report is an effective and promising approach for promoting photocatalytic performance of ZnO. This research offers a new avenue to capture and convert solar energy to remove organic pollutants in our environment. Regarding to the similar properties between graphene and CNT, ZnO-CNT hybrid could be also a potential photocatalyst with high performance [45]. We also carried out some research to study the photocatalytic activity of ZnO-CNT, and the results will be published in future.

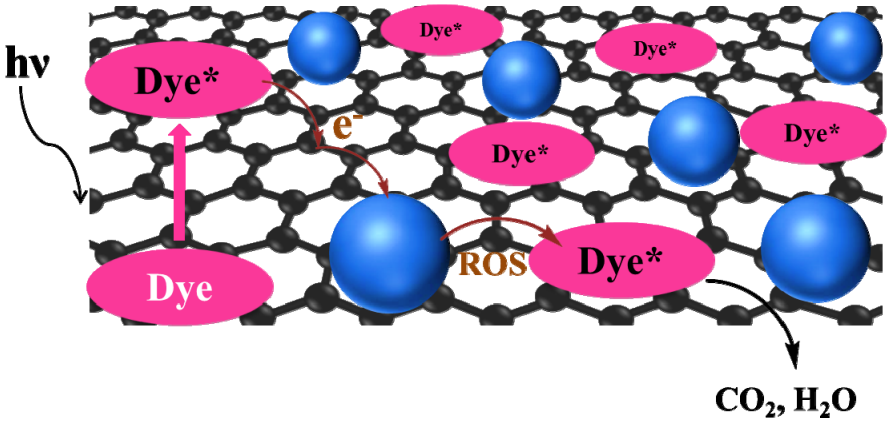

Figure 8. Proposed mechanism for the photocatalytic degradation of RhB by ZnO-RGO under visible light irradiation.

4. Conclusion

ZnO-RGO hybrids containing high loading of well-dispersed ZnO nanoparticles with an average diameter of 4.5 ± 0.5 nm have been successfully prepared via a one-step sol-gel method. It is found that the nanosized ZnO can hybridize with RGO and have efficient electrostatic interactions with RGO. The small particle size, great dye adsorptivity, and excellent electron transport properties from RGO make the ZnO-RGO an efficient and stable photocatalyst. The present study offers a low-cost, straightforward approach for fabricating nanostructured ZnO-RGO hybrids. It is expected that the current research can stimulate significant interest in the preparation of effective photocatalysts based on RGO and metal oxide hybrids, which finds attractive applications in tackling environmental pollution issues.

Acknowledgments

The authors would like to thank Kaneka Corporation for their financial support. Special thank is also given to Dr. Hongcai Zhou in Texas A&M University for surface area measurements.

Conflict of Interest

The authors declare no conflicts of interest regarding this paper.

References

1. Du J, Lai X, Yang N, et al. (2011) Hierarchically ordered macro-mesoporous TiO_2-graphene composite films: Improved mass transfer, reduced charge recombination, and their enhanced photocatalytic activities. *ACS Nano* 5: 590–596.
2. Li X, Wang Q, Zhao Y, et al. (2013) Green synthesis and photo-catalytic performances for ZnO-reduced graphene oxide nanocomposites. *J Colloid Interf Sci* 411: 69–75.
3. Zhang H, Lv X, Li Y, et al. (2010) P25-graphene composite as a high performance photocatalyst. *ACS Nano* 4: 380–386.
4. Wu TX, Liu GM, Zhao JC, et al. (1998) Photoassisted degradation of dye pollutants. V. Self-photosensitized oxidative transformation of Rhodamine B under visible light irradiation in aqueous TiO_2 dispersions. *J Phys Chem B* 102: 5845–5851.
5. Bannat I, Wessels K, Oekermann T, et al. (2009) Improving the photocatalytic performance of mesoporous titania films by modification with gold nanostructures. *Chem Mater* 21: 1645–1653.
6. Liang Y, Wang H, Casalongue HS, et al. (2010) TiO_2 nanocrystals grown on graphene as advanced photocatalytic hybrid materials. *Nano Res* 3: 701–705.
7. Li B, Cao H (2011) ZnO@graphene composite with enhanced performance for the removal of dye from water. *J Mater Chem* 21: 3346–3349.
8. Yu JC, Li GS, Wang XC, et al. (2006) An ordered cubic Im3m mesoporous Cr-TiO_2 visible light photocatalyst. *Chem Commun* 25: 2717–2719.
9. Han C, Yang MQ, Weng B, et al. (2014) Improving the photocatalytic activity and anti-photocorrosion of semiconductor ZnO by coupling with versatile carbon. *Phys Chem Chem Phys* 16: 16891–16903.
10. Zhang Q, Tian C, Wu A, et al. (2012) A facile one-pot route for the controllable growth of small sized and well-dispersed ZnO particles on GO-derived graphene. *J Mater Chem* 22: 11778–11784.
11. Han C, Zhang N, Xu YJ (2016) Structural diversity of graphene materials and their multifarious roles in heterogeneous photocatalysis. *Nano Today* 11: 351–372.
12. Zhang N, Yang MQ, Liu S, et al. (2015) Waltzing with the versatile platform of graphene to synthesize composite photocatalysts. *Chem Rev* 115: 10307–10377.
13. Yao H, Jin L, Sue HJ, et al. (2013) Facile decoration of Au nanoparticles on reduced graphene oxide surfaces via a one-step chemical functionalization approach. *J Mater Chem A* 1: 10783–10789.
14. Yao H, Huang TC, Sue HJ (2014) Self-assembly of Au nanoparticles on graphene sheets as a catalyst with controlled grafting density and high reusability. *RSC Adv* 4: 61823–61830.
15. Yin H, Tang H, Wang D, et al. (2012) Facile synthesis of surfactant-free Au cluster/graphene hybrids for high-performance oxygen reduction reaction. *ACS Nano* 6: 8288–8297.
16. Gao E, Wang W, Shang M, et al. (2011) Synthesis and enhanced photocatalytic performance of graphene-Bi_2WO_6 composite. *Phys Chem Chem Phy* 13: 2887–2893.
17. Zhang Y, Tang ZR, Fu X, et al. (2010) TiO_2-graphene nanocomposites for gas-phase photocatalytic degradation of volatile aromatic pollutant: Is TiO_2-graphene truly different from other TiO_2-carbon composite materials? *ACS Nano* 4: 7303–7314.

18. Zhang N, Xu YJ (2016) The endeavour to advance graphene-semiconductor composite-based photocatalysis. *Crystengcomm* 18: 24–37.
19. Yang MQ, Xu YJ (2016) Photocatalytic conversion of CO_2 over graphene-based composites: current status and future perspective. *Nanoscale Horiz* 1: 185–200.
20. Yang MQ, Zhang N, Pagliaro M, et al. (2014) Artificial photosynthesis over graphene-semiconductor composites. Are we getting better? *Chem Soc Rev* 43: 8240–8254.
21. Yang MQ, Han C, Zhang N, et al. (2015) Precursor chemistry matters in boosting photoredox activity of graphene/semiconductor composites. *Nanoscale* 7: 18062–18070.
22. Gao X, Jang J, Nagase S (2010) Hydrazine and thermal reduction of graphene oxide: Reaction Mechanisms, Product Structures, and Reaction Design. *J Phys Chem C* 114: 832–842.
23. Stankovich S, Dikin DA, Piner RD, et al. (2007) Synthesis of graphene-based nanosheets via chemical reduction of exfoliated graphite oxide. *Carbon* 45: 1558–1565.
24. Hung MC, Yuan SY, Hung CC, et al. (2014) Effectiveness of ZnO/carbon-based material as a catalyst for photodegradation of acrolein. *Carbon* 66: 93–104.
25. Moussa H, Girot E, Mozet K, et al. (2016) ZnO rods/reduced graphene oxide composites prepared via a solvothermal reaction for efficient sunlight-driven photocatalysis. *Appl Catal B-Environ* 185: 11–21.
26. Chen Z, Zhang N, Xu YJ (2013) Synthesis of graphene-ZnO nanorod nanocomposites with improved photoactivity and anti-photocorrosion. *Crystengcomm* 15: 3022–3030.
27. Li B, Liu T, Wang Y, et al. (2012) ZnO/graphene-oxide nanocomposite with remarkably enhanced visible-light-driven photocatalytic performance. *J Colloid Interf Sci* 377: 114–121.
28. Luo QP, Yu XY, Lei BX, et al. (2012) Reduced graphene oxide-hierarchical ZnO hollow sphere composites with enhanced photocurrent and photocatalytic activity. *J Phys Chem C* 116: 8111–8117.
29. Schoenhalz AL, Arantes JT, Fazzio A, et al. (2010) Surface and quantum confinement effects in ZnO nanocrystals. *J Phys Chem C* 114: 18293–18297.
30. Sun D, Sue HJ, Miyatake N (2008) Optical properties of ZnO quantum dots in epoxy with controlled dispersion. *J Phys Chem C* 112: 16002–16010.
31. Hoffmann MR, Martin ST, Choi WY, et al. (1995) Environmental applications of semiconductor photocatalysis. *Chem Rev* 95: 69–96.
32. Zhang Y, Chen Z, Liu S, et al. (2013) Size effect induced activity enhancement and anti-photocorrosion of reduced graphene oxide/ZnO composites for degradation of organic dyes and reduction of Cr(VI) in water. *Appl Catal B-Environ* 140: 598–607.
33. Sun D, Wong M, Sun L, et al. (2007) Purification and stabilization of colloidal ZnO nanoparticles in methanol. *J Sol-Gel Sci Techn* 43: 237–243.
34. Hummers WS, Offeman RE (1958) Preparation of graphitic oxide. *J Am Chem Soc* 80: 1339–1339.
35. Fan X, Peng W, Li Y, et al. (2008) Deoxygenation of exfoliated graphite oxide under alkaline conditions: A green route to graphene preparation. *Adv Mater* 20: 4490–4493.
36. Brus L (1986) Electronic wave-functions in semiconductor clusters-experiment and theory. *J Phys Chem* 90: 2555–2560.

37. Yao H, Chu CC, Sue HJ, et al. (2013) Electrically conductive superhydrophobic octadecylamine-functionalized multiwall carbon nanotube films. *Carbon* 53: 366–373.
38. Mu J, Shao C, Guo Z, et al. (2011) High photocatalytic activity of ZnO-carbon nanofiber heteroarchitectures. *ACS Appl Mater Inter* 3: 590–596.
39. Zhang Y, Zhang N, Tang ZR, et al. (2012) Graphene transforms wide band gap ZnS to a visible light photocatalyst. The new role of graphene as a macromolecular photosensitizer. *ACS Nano* 6: 9777–9789.
40. Bai X, Wang L, Zong R, et al. (2013) Performance enhancement of ZnO photocatalyst via synergic effect of surface oxygen defect and graphene hybridization. *Langmuir* 29: 3097–3105.
41. Liu J, Li X, Dai L (2006) Water-assisted growth of aligned carbon nanotube-ZnO heterojunction arrays. *Adv Mater* 18: 1740–1744.
42. Kuo FL, Li Y, Solomon M, et al. (2012) Workfunction tuning of zinc oxide films by argon sputtering and oxygen plasma: an experimental and computational study. *J Phys D-Appl Phys* 45: 065301–065307.
43. Weng B, Yang MQ, Zhang N, et al. (2014) Toward the enhanced photoactivity and photostability of ZnO nanospheres via intimate surface coating with reduced graphene oxide. *J Mater Chem A* 2: 9380–9389.
44. Zhang LW, Fu HB, Zhu YF (2008) Efficient TiO_2 photocatalysts from surface hybridization of TiO_2 particles with graphite-like carbon. *Adv Funct Mater* 18: 2180–2189.
45. Das R, Hamid SBA, Ali ME, et al. (2014) Multifunctional carbon nanotubes in water treatment: The present, past and future. *Desalination* 354: 160–179.

AIMS Press